Spectral Analysis of a Cylinder Wake Interacting with Coherent Structures in a Turbulent Boundary Layer

Elizabeth Torres De Jesús*, Palash Waghmare†, and Theresa Saxton-Fox‡
University of Illinois, Urbana-Champaign, Urbana, IL, 61801

The spectral and spatial behavior of the wake of a small cylinder immersed in a turbulent boundary layer at different wall-normal heights is studied and compared to a canonical turbulent boundary layer. Time-resolved particle image velocimetry measurements were taken downstream of the position where the cylinder is immersed. Measurements were also taken in of the unperturbed turbulent boundary layer in the same region without the cylinder for the same freestream velocity. The pre-multiplied energy spectra was computed for the seven cases and compared. Changes to the spectral content of the wake and of the boundary layer were observed for cases where the cylinder was nearer to the wall, while little interaction was observed for cases with the cylinder outside of the boundary layer thickness. Spectral proper orthogonal decomposition modes were calculated at wavelengths relevant to the wake vortex shedding and to the energetic turbulent structures and modifications to the modes were observed for cases with strong interaction. Vortex detection methods were used to visualize the wake and suggested that both a breakdown of periodicity of the vortex spacing and an overall spatial meandering of the wake may be responsible for the spectral modifications observed.

I. Nomenclature

G	=	wall-normal distance between bottom of the cylinder and wall
U_∞	=	freestream velocity
U_c	=	convection velocity
D	=	cylinder diameter
u_τ	=	friction velocity
δ	=	boundary layer thickness at 99% of freestream velocity
St	=	Strouhal number
Re_τ	=	friction Reynolds number
Re_D	=	Reynolds number based on cylinder diameter
y_c/δ	=	normalized wall-normal location of cylinder centerline
x_{LE}	=	streamwise distance from plate's leading edge
f	=	frequency
λ/δ	=	wavelength normalized in outer units
R_{uu}	=	time auto-correlation function of the streamwise velocity fluctuation
ϕ_{uu}	=	power spectral density of the streamwise velocity fluctuation
k_{xx}	=	wavenumber
L	=	modal energy
x, y	=	streamwise and wall-normal coordinates
u, v	=	streamwise and wall-normal velocities
ω_{RES}	=	residual vorticity

II. Introduction

The flow past a cylinder has been studied extensively both for incoming flows with uniform velocity [1–3] and for cylinder immersed in non-uniform flows such as a boundary layers [4–10]. At sufficiently high Re_D for cylinders

*Graduate Research Assistant, Department of Aerospace Engineering, 104 S Wright Street., AIAA Student Member
†Graduate Research Assistant, Department of Aerospace Engineering, 104 S Wright Street.
‡Assistant Professor, Department of Aerospace Engineering, 104 S Wright Street, and AIAA Member

immersed in uniform flows, coherent vortex shedding is observed in the wake of a cylinder with a predictable and repeatable Strouhal number, St [5]. The current study focuses on a cylinder immersed in a turbulent boundary layer. This configuration introduces a number of additional complexities and non-dimensional numbers. The presence of a wall, regardless of the boundary layer dynamics, modifies the behavior of the wake. The gap ratio, G/D, between the cylinder and the wall significantly affects the wake dynamics. Bearman and Zdravkovich [11] observed the suppression of regular vortex shedding when $G/D < 0.3$ for the bottom part of the cylinder, while it remained regular if G/D was above this value. Other studies have also noted that $G/D = 0.25 - 0.5$ is a critical value for which near-wall vortex suppression happens in the range $Re_D = 1.2 - 4.8 \times 10^4$.

The presence of the cylinder itself can also modify the turbulent boundary layer dynamics, with a dependence on the ratio between the size of the cylinder and the thickness of the boundary layer. Sarkar and Sarkar [8] highlighted the implications for the boundary layer statistics of placing a cylinder in a boundary layer. The boundary layer was observed for be deflected away from the wall and a separation bubble formed upstream and downstream of the cylinder. In addition, the boundary layer was observed to modify the cylinder flow, showing changes to St as well as lift and drag coefficients of the cylinder. Marumo et al. [6] experimentally studied the cylinder in a turbulent boundary layer with $D/\delta = 0.3$, and $y_c/\delta = 0.222, 0.556, 1.24$. They found that the boundary layer recovered faster for lower heights of the cylinder and also showed effects in the skin friction coefficient, with increases close to the cylinder followed by constant regions and slow decrease with streamwise distance for the latter two cases. This connects with later findings using large-eddy breakup devices, some of them being cylinders, where they were placed in the outer region of the turbulent boundary layer and a decrease in skin friction was observed [12–15]. The decrease in skin friction was suggested to be due to an effect on the coherent structures that exist in the outer region of the turbulent boundary layer [16, 17], which also in turn modifies the small-scale structures in the order of viscous units near the wall [18] .

The interaction of the cylinder wake and the turbulent boundary layer can also be thought of in the context of the interaction of the coherent structures associated with both flows. Within the wake flow community, such interactions have previously been studied in the context of wind turbines, where wind turbine wakes have been observed to be advected and meander because of the influence of passing large-scale turbulent structures [19]. Within the context of the turbulent boundary layer community, interactions between large-scale coherent structures and small-scale structures have been observed by different works through techniques including amplitude and frequency modulation [20–22] as well as conditional averaging that has highlighted height variation [23–25].

In the current work, we study a cylinder wake interacting with a turbulent boundary layer using time-resolved particle image velocimetry, allowing us to study the structural behavior of the wake and the boundary layer as well as the frequency dynamics. We focus on a small cylinder with a relatively large gap ratio, such that separation does not occur in the boundary layer and such that the cylinder vortex structures are sized to be overlapping with the small-scale frequencies in the outer region of the boundary layer in which it is placed. The manuscript shows results for the pre-multiplied spectra and thespectral proper orthogonal decomposition of the flow field, to gain insight into the modifications to both the wake and the boundary layer that arises through their interaction. In addition, vortex tracking is used to offer hypotheses about the origin of spectral changes, including from modification of spacing of vortices as the wake evolves downstream, and from the overall meandering of the cylinder wake.

III. Data Acquisition

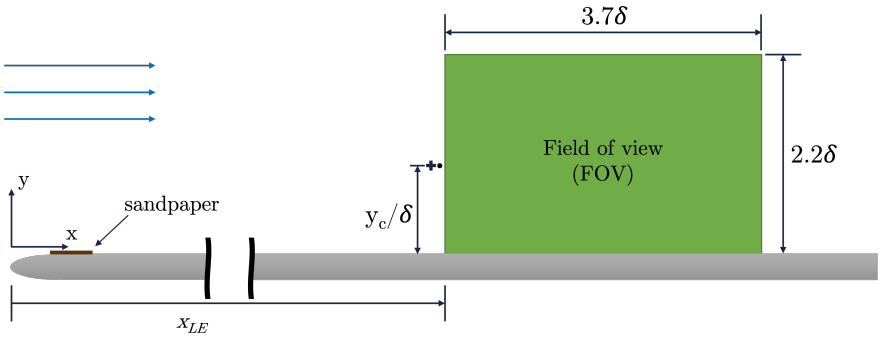

Fig. 1 Experimental Setup Schematic.

A series of experiments were conducted at the Aerodynamics Research Laboratory at University of Illinois, Urbana-Champaign. In these experiments, a cylinder (D/δ=0.05) was placed over a flat plate at six wall-normal locations $y_c/\delta = 0.36, 0.45, 0.59, 0.78, 0.89, 1.09$ (G/D= 7.02, 8.9, 11.8, 15.8, 18.1, 21.8) with its axis along the span of the plate. Measurements were also taken in the same field of view without the cylinder immersed as a baseline turbulent boundary layer case. The region of the measurements started at x_{LE} = 2.27m, where δ = 39.8mm, yielding $Re_\tau = u_\tau\delta/\nu \approx 1000$ and $Re_D = 1100$. For the experimental configuration, see Fig. 1. Time-resolved and non time-resolved two-dimensional Particle Image Velocimetry was used to obtain velocity field measurements starting just downstream of the cylinder location at sampling rates of 3755 Hz and 100 Hz respectively with a field of view of $3.7\delta \times 2.2\delta$ in the streamwise-wall-normal plane as presented on Fig. 1, yielding 6170 snapshots for each temporal resolution. A single Phantom VEO710L High-Speed Camera was used with resolution of 1280×800 pixels, which yielded an interrogation window with a spatial resolution of 1.88mm × 1.94mm, equivalent to 43.19×44.57 viscous units or $0.0472\delta \times 0.0487\delta$. The wind tunnel free-stream velocity was held at U_∞ = 9.3 m/s for all tests in this work. The freestream turbulence intensity was observed to be 1% or lower.

IV. Methodology

A. Pre-multiplied Spectra

The energy spectral density is evaluated for all the cases with the cylinder present as well as the case with nothing immersed in the turbulent boundary layer. The calculation is performed for all wall-normal heights, y, at a streamwise position $x/\delta = 1.98$ downstream of the cylinder by taking the Fourier transform of the time auto-correlation, in this instance of the streamwise velocity fluctuation, such that

$$\phi_{uu}(\omega) = \frac{1}{2\pi}\int_{-\infty}^{\infty} e^{i\omega t} R_{uu}(t)\, dt. \tag{1}$$

The power spectral density ϕ_{uu} is obtained using Welch's method, where the time-series of the streamwise velocity is split into overlapping segments and windowed. For this case, 50% overlap over 50 windows is done and with this we can find $k = \frac{2\pi f}{U_c}$, where f is obtained through Welch's method and U_c is the mean streamwise velocity at the location where the spectral analysis is being done following Taylor's hypothesis. Based on this, the pre-multiplied spectra $\frac{k_{xx}\phi_{uu}}{u_\tau^2}$ is calculated and shown for all cases y_c/δ and the turbulent boundary layer case on Fig. 3(a-g). Additionally, a wavelength is identified as relevant for large-scale structures in the turbulent boundary layer, $\lambda/\delta \approx 7$ and highlighted with dashed lines in Fig. 3.

B. Spectral Proper Orthogonal Decomposition (SPOD)

The cases are analyzed to look further into the modes associated with certain frequencies using SPOD [26]. This spectral analysis allows for isolating the spatio-temporally coherent modes at each frequency encountered in the cases. Through this form of proper orthogonal decomposition, an optimal orthogonal basis for a data set is to be found, which captures the largest part of the total energy contained. With the assumption of statistically stationary data, SPOD yields modes which are orthogonal under a space-time inner product and therefore express spatiotemporal coherence. The resulting modes with this technique are the eigenvectors of the cross spectral density at each frequency extracted from the data. Because this present study includes data that has non-zero mean, the fluctuating velocity is used to obtain the modes on each of the cases. The results for the modal energy and the first two modes associated with f_s for all cylinder cases are presented in Figs. 4 and 5 respectively.

V. Results

The instantaneous streamwise velocity fields for the cases $y_c/\delta = 0.36$ (a), $y_c/\delta = 0.59$ (b), $y_c/\delta = 1.09$ (c), and without a cylinder (d) are shown in Fig. 2. These instantaneous visualizations are provided to give a sense for the ratio of scales and the extent of interaction for the different cases. In Fig. 2(a) and (b), the cylinder deep enough in the boundary layer to suggest significant interactions between the two flows, while less interaction would be expected in Fig. 2(c) due to the distance between the cylinder and the wall, though some interaction is still suggested by the figure, especially when the large-scale turbulent bulges extend farther from the wall than on average. The intensity of the wake can also be seen to be fairly dominant, overpowering the existing local coherent structures in the visualizations, especially in cases with the cylinder nearer to the wall.

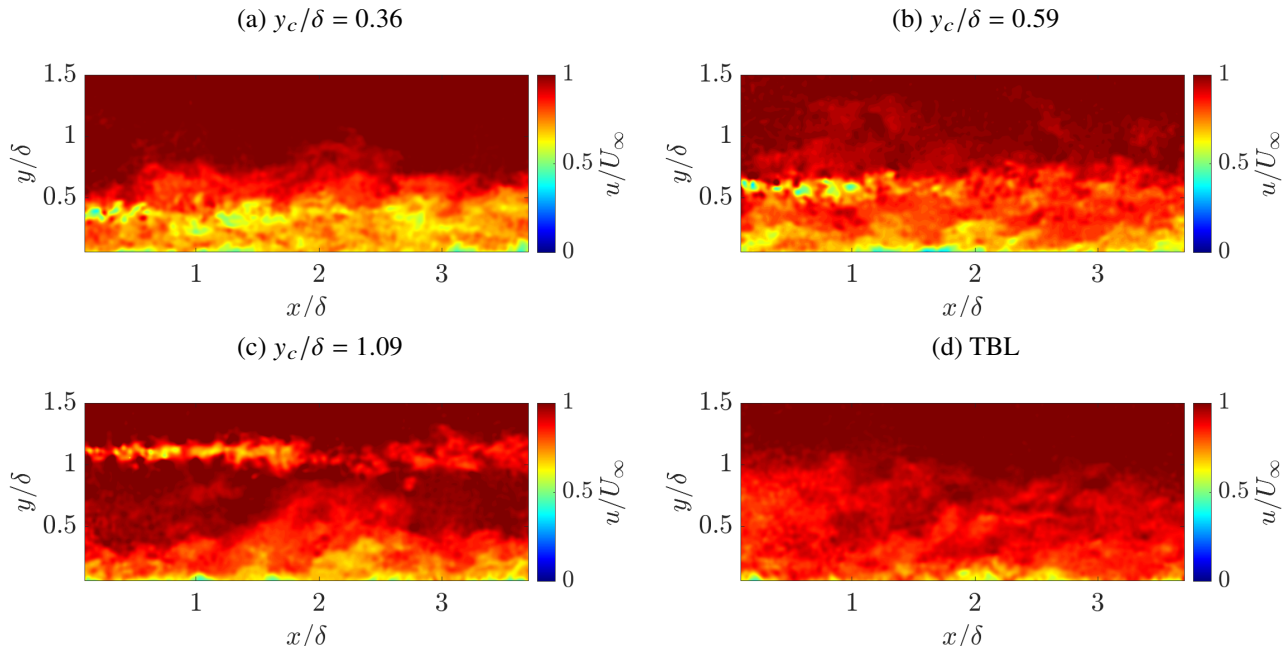

Fig. 2 Instantaneous streamwise velocity fields for cases y_c/δ = 0.36 (a), 0.59 (b), 1.09 (c), and TBL (d) normalized by U_∞.

Calculating the pre-multiplied spectra for the cases studied helps draw comparisons in the spectral content of the flow and how this is changing when imposing the cylinder at different wall-normal locations. The pre-multiplied spectra for turbulent boundary layers has been extensively studied, and the results shown in Fig. 3(g) show qualitative agreement with the expected energetic frequencies. For example, a peak at longer wavelengths (superstructures) in the outer region of the boundary layer is observed [20, 27] corresponding to $\lambda/\delta \approx 7$, highlighted with an orange dashed line.

Inspecting the pre-multiplied spectra, it is seen that frequencies that are energetic in the unperturbed turbulent boundary layer are modified by the presence of the cylinder depending on the cylinder height, and is also seen that there are dynamics between the cylinder and the turbulent boundary layer that become pertinent. In Figs. 3(a-f), connections between the location of the cylinder and the overall spectral signature associated with the turbulent boundary layer can be made. For the first three cases, Fig. 3(a-c), there is a similar behavior with regards to the location of the cylinder. For these three cases, above the cylinder location, there appears to be higher amplitude along a wide range of the shorter wavelength content. The wavelength expected to be associated with the Strouhal number of vortex shedding is highlighted with a red dashed line. For the three cases nearest to the wall, a range of frequencies at larger wavelength than the expected Strouhal number are observed to be energetic. These wavelengths also show evidence of localization at a height farther from the wall than the center of the cylinder. The center of the cylinder is visualized in each case with a white dashed line. The shift to heights above the cylinder heights and the shift of frequencies to larger frequencies than the traditional Strouhal number might both suggest that the vortices on the underside of the cylinder, which would be associated with vorticity that swirls contrary to the direction of the mean shear, might be weakened while the vortices on the topside of the cylinder may have been strengthened. The increase in energy at larger wavelengths in the wake may also suggest interaction with longer wavelength turbulent boundary layer structures. As the cylinder is moved farther from the wall, for example in Fig. 3(d-f), the energy of the cylinder wake is more centered at the height of the cylinder and shows more localization at the expected Strouhal number. These observations may suggest less asymmetric suppression of the underside and amplification of the upperside vortices in the cylinder wake, as well as suggesting less interaction overall with the turbulent boundary layer.

The turbulent boundary layer spectra also shows evidence of modification due to the presence of the cylinder. The colorbar of the spectra are held constant across all the panels in Fig. 3, and the height at which the boundary layer structures remain energetic is observed to be higher for cases without a cylinder or with a cylinder farther from the wall. For the near-wall cases, for example Fig. 3(a-c), significant suppression of the turbulent spectra is observed below the cylinder height, particularly at long wavelengths over $\lambda_x \approx 2\delta$. There appears to be more energetic activity at shorter

wavelengths in the boundary layer, particularly for the case $y_c/\delta = 0.36$ in Fig. 3(a).

For all the cases presented in Section III, the modal energies L obtained for each case are plotted against the frequencies extracted along with the 99% confidence bounds in Fig. 4. For all cases, there is a peak at the high frequency end of the frequencies extracted for each case. This frequency is associated with the shedding frequency of the cylinder for each instance. This peak and overall L varies for each case. Similarly to the observations made of the pre-multiplied spectra (Fig. 3), the trends of the cases can be divided by what happens to the three cases closest to the wall and the three that are farthest. The peak corresponding to f_s for $y_c/\delta = 0.36$ (4(a)) presents the broadest spread of all cases, with this spread decreasing with increasing y_c/δ presented in Figs. 4(b-f). For the three cases farthest from the wall, Figs. 4(d-f), there is the appearance of a secondary peak at very high frequencies.

From the modal energies shown in Fig. 4, the frequency at which each of the principal peaks happen for the cylinder cases in the higher range is chosen and the first two spectral proper orthogonal decomposition (SPOD) modes are shown. These two SPOD modes for each y_c/δ are shown in Fig. 5, where the cylinder location is presented with a dashed line. The first mode, shown on the left column for Fig. 5, presents as a wavepacket that remains coherent and prevails until around $x \approx \delta$, which somewhat varies for each case. For the cases $y_c/\delta = 0.36, 0.45, 0.59$, shown in Figs. 5(a-c), the wavepacket decays below its upstream value at around $0.7 - 0.8\delta$ for that first mode. Conversely, for the first mode of the cases shown in Figs. 5(d-f), $y_c/\delta = 0.78, 0.89, 1.09$, the wavepacket starts prevailing for slightly longer than the previous cases. It appears that the case $y_c/\delta = 0.59$, Fig. 5(c), is the one presenting the first signs of this change to that first mode. The case that prevails most is $y_c/\delta = 1.09$, Fig. 5(f), which stops slightly beyond $x = \delta$. The behavior of this first mode appears consistent with what happens near the cylinder, where the frequency associated with the cylinder is strongest. However, as the wake evolves downstream, it interacts with other structures in the flow, which in this case are the coherent structures present in the turbulent boundary layer, which influences the loss of energy of that first mode.

The second mode for all cylinder cases, presented on the right column of Fig. 5, presents interesting dynamics. The first aspect that is shared across all cases is that the second mode appears as a wavepacket as well. Nevertheless, this wavepacket appears less coherent even though its energy lasts beyond $x = \delta$. For the second mode of $y_c/\delta = 0.36$, Fig. 5(a), the second mode persists across the streamwise extent for the whole field of view even though with less energy beyond $x = \delta$, and it remains with more intensity above the cylinder than below it. It also presents an asymmetric distribution with respect to the cylinder centerline and in the region between $x = 1 - 2\delta$ there is a weak packet that tends towards the wall. Starting with the case $y_c/\delta = 0.45$, Fig. 5(b), the second mode appears to show more symmetry with respect to the centerline than the case before. It also maintains a weak packet that persists across the streamwise extent of the current field of view. These trends, however, appear to change with the case $y_c/\delta = 0.59$, Fig. 5(b), where the second mode appears to lose energy by $x = 1.5\delta$. After this case, the second mode for the cases $y_c/\delta = 0.78, 0.89, 1.09$, Figs. 5(d-f), shows to remain stronger for longer, extending for almost $x = 2\delta$, with the case $y_c/\delta = 1.09$ showing more symmetry with respect to the cylinder.

The SPOD results present observations that could show connections to the pre-multiplied spectra presented in Fig. 3. Even though in the SPOD first mode Fig. 5 for $f = f_s$, persists until $x = \delta$ in the streamwise extent for all the cases and starts decaying afterwards, on the other hand, when the pre-multiplied spectra is taken, which in Fig. 3 is shown for $x = 1.98\delta$, there is still a signature present related to the vortices being shed by the cylinder. As previously discussed, in the pre-multiplied spectra the presence of the cylinder at the different wall-normal locations appears to affect the energy across the different wavelengths, and based on the evidence presented by the first two SPOD modes that this effect could possibly be due to more than the shedding frequency itself. That is, the dominance of the shedding does not prevail for too long in the streamwise extent as the height of the cylinder is decreased. Based on this, the first mode associated with the frequency of wavelength $\lambda/\delta \approx 7$ is plotted in Fig. 6 for all the cylinder cases as well as the turbulent boundary layer.

In the first mode presented in Fig. 6 it can be seen that the main structure for all cases extends from the bottom of wall-normal extent and covers most of the wall-normal region until $y \approx \delta$. For the cases $y_c/\delta = 0.36, 0.45, 0.59$, Figs. 6(a-c), a clear streak across these structures that coincides with the cylinder location on each instance is present. This appears to weaken the structure in this first mode for all three cases. In the case in Fig. 6(c), where $y_c/\delta = 0.59$, this streak goes along with more intensity below the structure and weakening in the part above it. Same thing appears to happen for the case $y_c/\delta = 0.78$, shown in Fig. 6(d). This observation is similar from what is observed in the pre-multiplied spectra, where overall this wavelength appears weakened differently for each cylinder location.

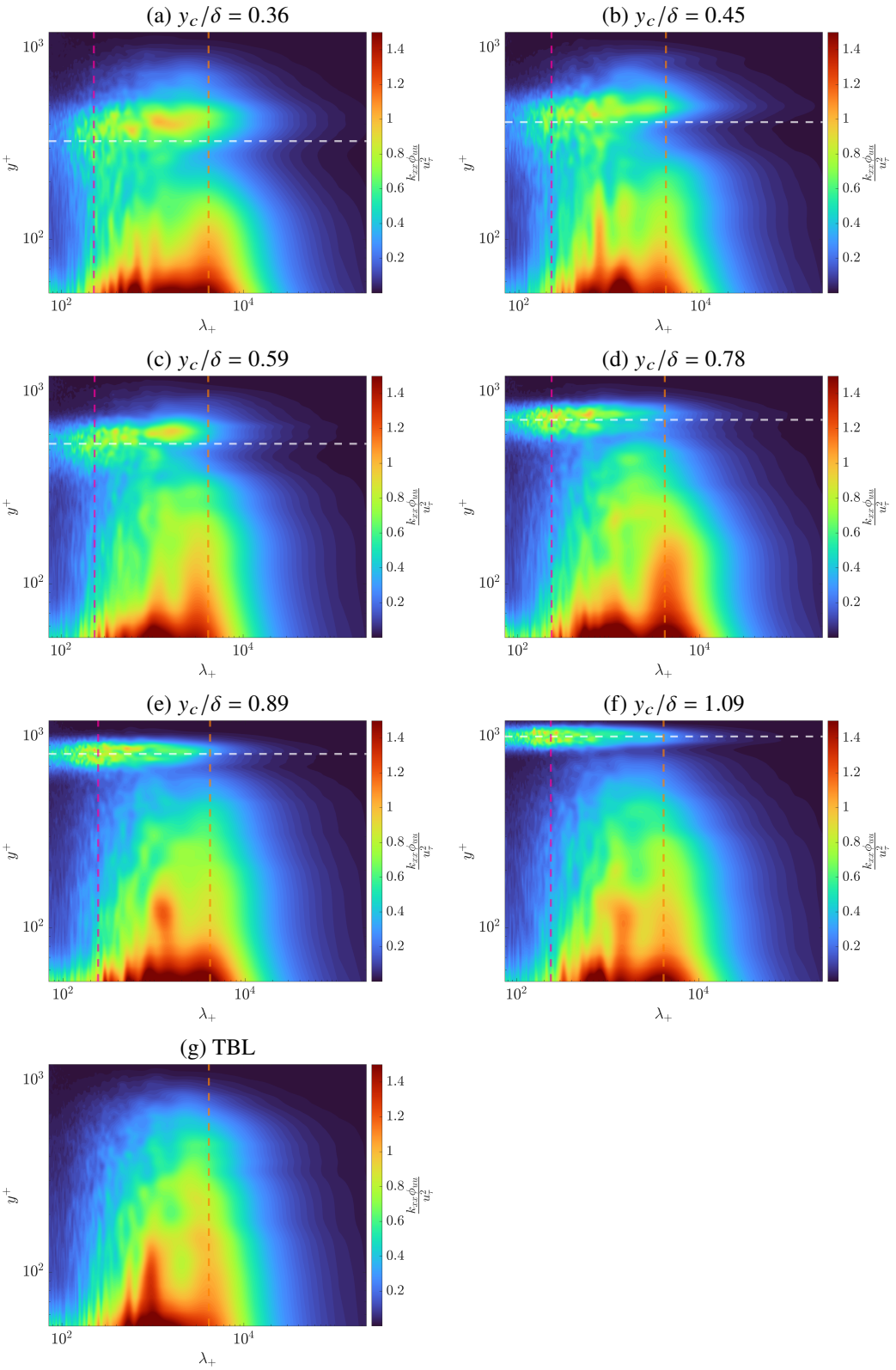

Fig. 3 Pre-multiplied spectra $\frac{k_{xx}\phi_{uu}}{U_\tau^2}$ at $x/\delta = 1.94$. The horizontal white dashed line shows y_c/δ for each case. The dashed vertical lines are select wavelengths equivalent to f_s for each y_c/δ (dark pink) and $\lambda/\delta \approx 7$ (orange).

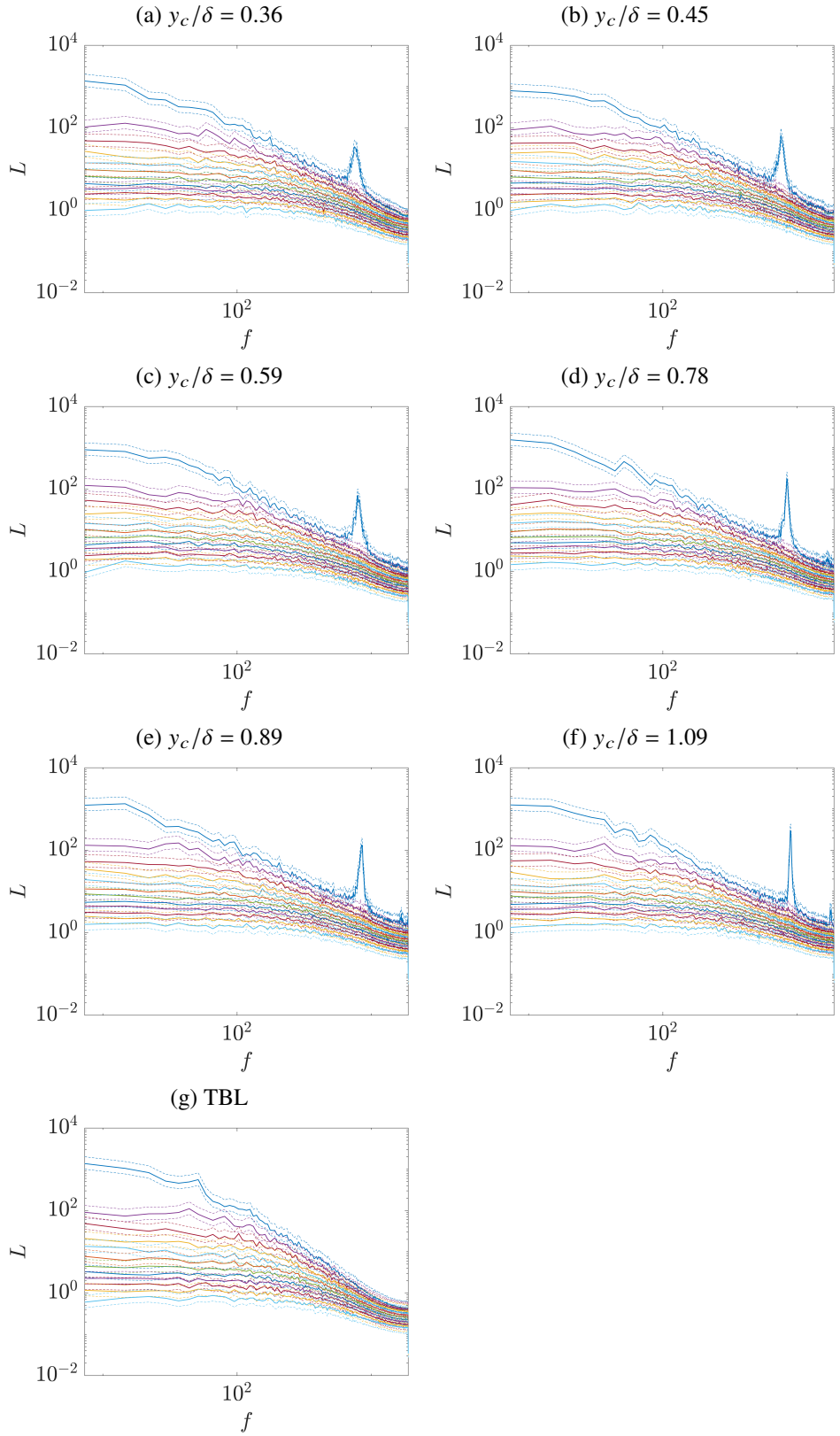

Fig. 4 Modal energy and 99% confidence bounds (shown with dashed lines) vs frequency

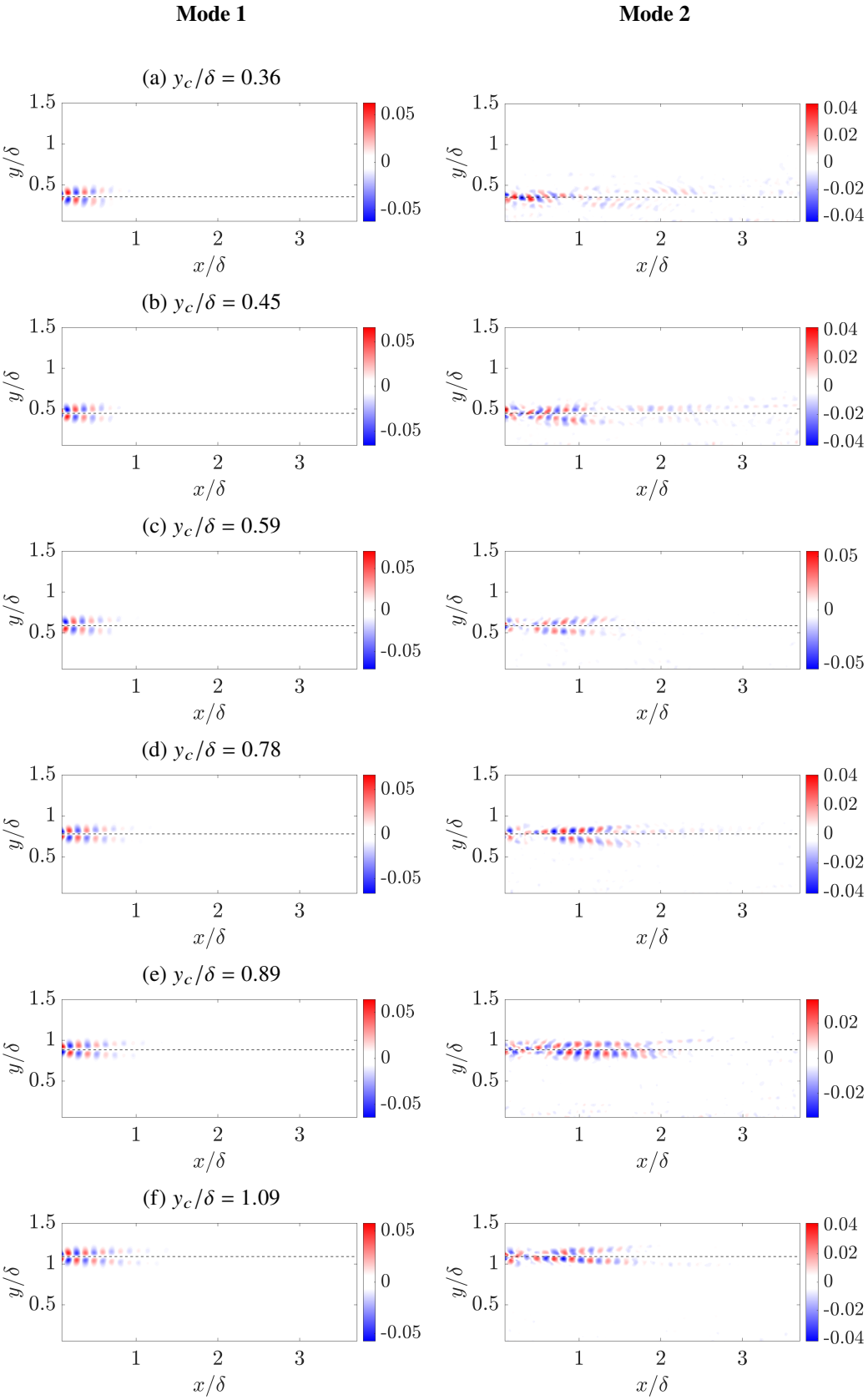

Fig. 5 First mode (left column) and second mode (right column) for $f = f_s$. The dashed line indicates the cylinder location.

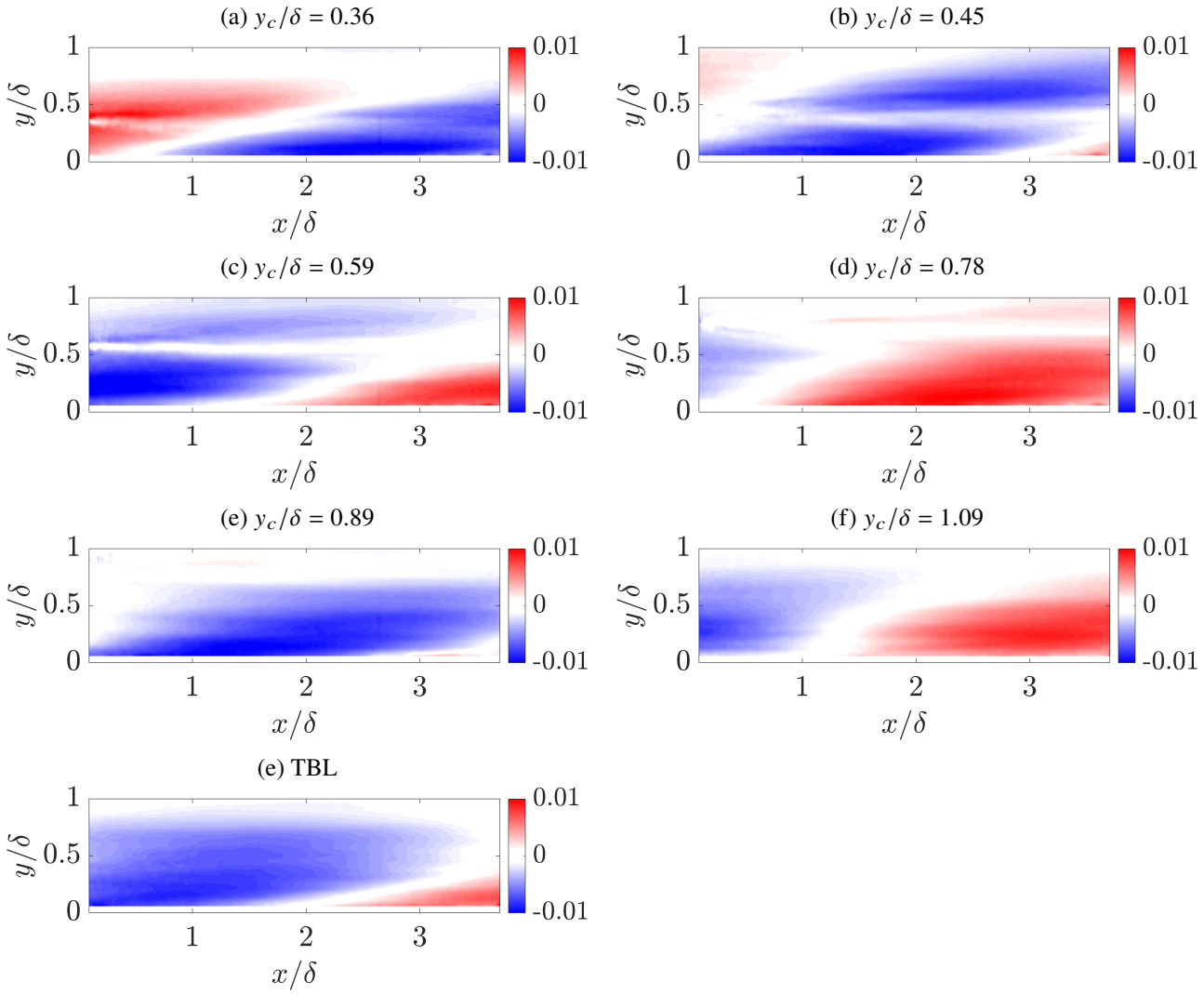

Fig. 6 First SPOD mode for the frequency associated with $\lambda/\delta \approx 7$ for each y_c/δ and the TBL case.

To complement the frequency-based analyses of the prior sections, the wake was also analyzed using vortex identification methods. Spanwise vortices were identified in the field of view using the triple decomposition method (TDM), which decomposes the velocity gradient tensor into shearing, straining, and swirling motions. The triple decomposition method has previously been shown to provide a better representation of vortex rotation when vortices are embedded in shear flows than the swirling strength [28]. The residual vorticity in a specific snapshot in time is shown in Fig. 7(a). A threshold value of residual vorticity was identified and any points with sufficiently high residual vorticity were marked as shown in Fig. 7(b). Note that multiple points clustered together can indicate a single large vortex in the current implementation. The case shown in Fig. 7 is one in which the cylinder is embedded in the boundary layer and the threshold is chosen to primarily highlight wake vortex activity.

It is hypothesized that the broadening of the vortex shedding frequency peak observed in the spectra of Fig. 4 can be attributed both to a breakdown in the periodicity of the wake as well as to a meandering of the wake, as has been observed in wind turbine studies. Both effects are visible by eye in Fig. 7. The regularity of observed vortices in the snapshot shown breaks down starting around $x \approx 2\delta$. True periodicity also immediately seems to break down, with essentially no vortices that counter the mean shear surviving in the field of view. Meandering of the full wake also appears to start rapidly, which is drawn out in Fig. 7(c) with a fitted curve attempting to fit the location of the wake vortices. While imperfect, the fitted curve highlights that the wake's central height changes rapidly in space as the wake is advected downstream. Prior work has suggested that the height of coherent vortices is associated with the presence of specific phases of coherent structures in the turbulent boundary layer that pass by the cylinder and have positive or negative vertical velocity components [23, 24]. The meandering of the wake when the cylinder is sufficiently low in the boundary layer that it feels the impact of these coherent structures is suggested to affect the apparent frequency content and coherence of the wake, yielding the variation in coherence observed in the first and second modes of the vortex shedding frequency across the cylinder heights (Fig. 5), as well as the breadth or narrowness of the peak of the vortex shedding frequency (Fig. 4).

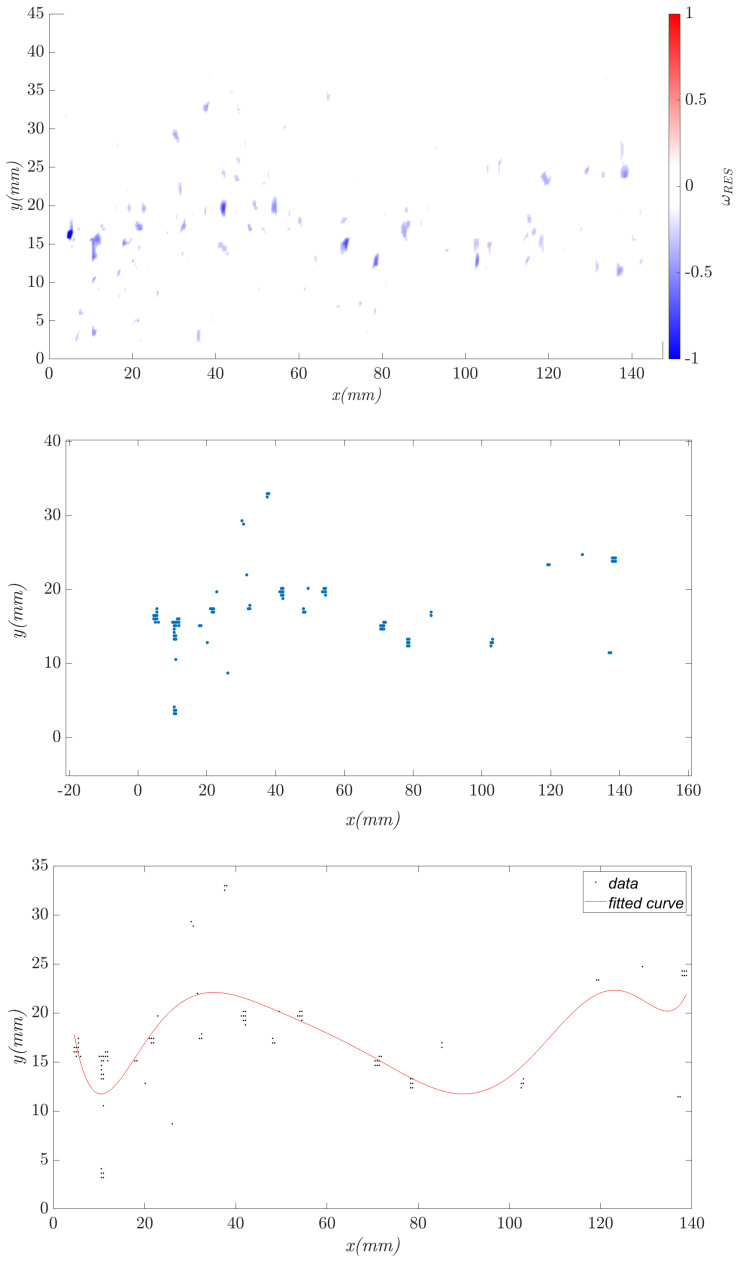

Fig. 7 Residual vorticity from the triple decomposition method (a) and points that surpass the threshold of residual vorticity (b). A curve fitted to the points of (b) is shown in (c) to highlight the meandering nature of the wake. x and y axes are shown in terms of mm.

VI. Conclusion

A cylinder was immersed in a turbulent boundary layer at six heights and the spectral content of the downstream flow was analyzed. The cylinder was chosen to generate coherent vortex shedding with a characteristic frequency associated with the smallest scales in the outer region of the turbulent boundary layer. For the nearest three cylinder cases, $y_c/\delta = 0.36, 0.45, 0.59$, the cylinder wake and the turbulent boundary layer were observed to significantly affect each other in the pre-multiplied energy spectra. The height where the dominant wake frequencies were observed was farther from the wall than the central height in the cylinder for these three cases. The frequencies that were observed to be most energetic in the cylinder wake in the pre-multiplied energy spectra were shifted to longer wavelengths than would be predicted from traditional Strouhal number predictions. And the turbulent boundary layer spectrum showed evidence of large-scale structure suppression at and below the cylinder wake height, and augmentation of small-scale structure energy at and below the cylinder wake height. For the three farthest cylinder cases, $y_c/delta = 0.78, 0.89$, and 1.09, much less evidence of interaction was observed in the pre-multiplied energy spectra. The cylinder wake showed a localization of energy at the cylinder height, with the most energetic frequencies close to that expected from traditional Strouhal number predictions. The turbulent boundary layer spectrum showed little change at large or small wavelengths.

Spectral proper orthogonal decomposition was performed on the flow field. The spectral energy of each mode was plotted, and a clear peak in the frequency content was observed for the first mode at a frequency at the vortex shedding frequency. This frequency peak was observed to be broader for cases with the cylinder nearer to the wall, and narrower for cases with the cylinder placed farther from the wall. The first two modes associated with the vortex shedding frequency were observed to decay in the streamwise direction, with a stronger decay for the cases nearer to the wall. The spectral POD mode for the large wavelength turbulent structure was also analyzed. Significant deformation and breakup was observed at the cylinder height for the three cases with the cylinder nearer the wall. Finally, the wake was visualized using a vortex identification method. The wake was observed to be less regular or periodic, and to exhibit significant meandering in the wall-normal direction. Both effects were hypothesized to affect the spectral signature of the wake.

References

[1] Roshko, A., "On the drag and shedding frequency of two-dimensional bluff bodies," Tech. Rep. No. NACA-TN-3169, 1954.

[2] Williamson, C. H., and Roshko, A., "Vortex formation in the wake of an oscillating cylinder," *Journal of Fluids and Structures*, Vol. 2, No. 4, 1988, pp. 355–381.

[3] Roshko, A., "Perspectives on bluff body aerodynamics," *Journal of Wind Engineering and Industrial Aerodynamics*, Vol. 49, 1993, pp. 79–100. https://doi.org/10.1016/0167-6105(93)90007-B.

[4] Taneda, S., "Experimental investigation of vortex streets," *Journal of the Physical Society of Japan*, Vol. 20, No. 9, 1965, pp. 1714–1721.

[5] Williamson, C. H., "Vortex Dynamics in the Cylinder Wake," *Annual Review of Fluid Mechanics*, Vol. 28, No. 1, 1996, pp. 477–539.

[6] Marumo, E., Suzuki, K., and Sato, T., "A turbulent boundary layer disturbed by a cylinder," *Journal of Fluid Mechanics*, Vol. 87, 1978, pp. 121–141. https://doi.org/10.1017/S0022112078002967.

[7] Sarkar, S., and Sarkar, S., "Large-Eddy Simulation of Wake and Boundary Layer Interactions Behind a Circular Cylinder," *Journal of Fluids Engineering, Transactions of the ASME*, Vol. 131, 2009, pp. 0912011–09120113. https://doi.org/10.1115/1.3176982.

[8] Sarkar, S., and Sarkar, S., "Vortex dynamics of a cylinder wake in proximity to a wall," *Journal of Fluids and Structures*, Vol. 26, No. 1, 2010, pp. 19–40.

[9] Zhou, J., Qiu, X., Li, J., and Liu, Y., "The gap ratio effects on vortex evolution behind a circular cylinder placed near a wall," *Physics of Fluids*, Vol. 33, 2021. https://doi.org/10.1063/5.0039611.

[10] Zhou, J., Qiu, X., Li, J., and Liu, Y., "Vortex evolution of flow past the near-wall circular cylinder immersed in a flat-plate turbulent boundary layer," *Ocean Engineering*, Vol. 260, 2022. https://doi.org/10.1016/j.oceaneng.2022.112011.

[11] Bearman, P. W., and Zdravkovich, M. M., "Flow around a circular cylinder near a plane boundary," *Journal of Fluid Mechanics*, Vol. 89, 1978, pp. 33–47. https://doi.org/10.1017/S002211207800244X.

[12] Chin, C., Örlü, R., Monty, J., Hutchins, N., Ooi, A., and Schlatter, P., "Simulation of a Large-Eddy-Break-Up Device (LEBU) in a Moderate Reynolds Number Turbulent Boundary Layer," *Flow, Turbulence and Combustion*, Vol. 98, 2017, pp. 445–460.

[13] Zheng, S., and Longmire, E. K., "Perturbing vortex packets in a turbulent boundary layer," *Journal of Fluid Mechanics*, Vol. 748, 2014, pp. 368–398. https://doi.org/10.1017/jfm.2014.185.

[14] Tan, Y. M., and Longmire, E. K., "Recovery of vortex packet organization in perturbed turbulent boundary layers," *Physical Review Fluids*, Vol. 2, No. 10, 2017, p. 104602.

[15] Corke, T. C., and Thomas, F. O., "Active and Passive Turbulent Boundary-Layer Drag Reduction," *AIAA Journal*, Vol. 56, No. 10, 2018, pp. 3835–3847.

[16] Kline, S. J., Reynolds, W. C., Schraub, F. A., and Runstadler, P. W., "The structure of turbulent boundary layers," *Journal of Fluid Mechanics*, Vol. 30, No. 4, 1967, pp. 741–773. https://doi.org/10.1017/s0022112067001740.

[17] Robinson, S. K., "Coherent Motions in the Turbulent Boundary Layer," *Annual Review of Fluid Mechanics*, Vol. 23, No. 1, 1991, pp. 601–639.

[18] Jimenez, J., and Moin, P., "The minimal flow unit in near-wall turbulence," *Journal of Fluid Mechanics*, Vol. 225, 1991, pp. 213–240. https://doi.org/10.1017/s0022112091002033.

[19] Larsen, G. C., Aagaard Madsen, H., and Bingöl, F., "Dynamic wake meandering modeling," 2007.

[20] Hutchins, N., and Marusic, I., "Large-scale influences in near-wall turbulence," *Philosophical Transactions of the Royal Society A: Mathematical, Physical and Engineering Sciences*, Vol. 365, No. 1852, 2007, pp. 647–664.

[21] Hutchins, N., and Marusic, I., "Evidence of very long meandering features in the logarithmic region of turbulent boundary layers," *Journal of Fluid Mechanics*, Vol. 579, 2007, pp. 1–28. https://doi.org/10.1017/S0022112006003946, URL https://doi.org/10.1017/S0022112006003946.

[22] Ganapathisubramani, B., Hutchins, N., Monty, J. P., Chung, D., and Marusic, I., "Amplitude and frequency modulation in wall turbulence," *Journal of Fluid Mechanics*, Vol. 712, 2012, pp. 61–91. https://doi.org/10.1017/jfm.2012.398.

[23] Saxton-Fox, T., Lozano-Durán, A., and McKeon, B. J., "Amplitude and wall-normal distance variation of small scales in turbulent boundary layers," *Physical Review Fluids*, Vol. 7, 2022. https://doi.org/10.1103/PhysRevFluids.7.014606.

[24] Shrivastava, S., and Saxton-Fox, T., "Correlation between Large-Scale Streamwise Velocity Features and the Height of Coherent Vortices in a Turbulent Boundary Layer," *Fluids*, Vol. 6, No. 8, 2021, p. 286.

[25] Chung, D., and McKeon, B., "Large-eddy simulation of large-scale structures in long channel flow," *Journal of Fluid Mechanics*, Vol. 661, 2010, pp. 341–364.

[26] Schmidt, O. T., and Colonius, T., "Guide to Spectral Proper Orthogonal Decomposition," *AIAA Journal*, Vol. 58, 2020, pp. 1023–1033. https://doi.org/10.2514/1.J058809.

[27] Mathis, R., Hutchins, N., and Marusic, I., "Large-scale amplitude modulation of the small-scale structures in turbulent boundary layers," *Journal of Fluid Mechanics*, Vol. 628, 2009, pp. 311–337. https://doi.org/10.1017/S0022112009006946.

[28] Kolář, V., "Vortex identification: New requirements and limitations," *International journal of heat and fluid flow*, Vol. 28, No. 4, 2007, pp. 638–652.